Nonlinear Structural Mechanics Based Modeling of Carbon Nanotube Deformation

Antonio Pantano, Mary C. Boyce, and David M. Parks*

Department of Mechanical Engineering, Massachusetts Institute of Technology, Cambridge, Massachusetts 02139-4307, USA

(Received 27 May 2003; published 3 October 2003)

A nonlinear structural mechanics based approach for modeling the structure and the deformation of single-wall and multiwall carbon nanotubes (CNTs) is presented. Individual tubes are modeled using shell finite elements, where a specific pairing of elastic properties and mechanical thickness of the tube wall is identified to enable successful modeling with shell theory. The effects of van der Waals forces are simulated with special interaction elements. This new CNT modeling approach is verified by comparison with molecular dynamics simulations and high-resolution micrographs available in the literature. The mechanics of wrinkling of multiwall CNTs are studied, demonstrating the role of the multiwalled shell structure and interwall van der Waals interactions in governing buckling and postbuckling behavior.

DOI: 10.1103/PhysRevLett.91.145504 PACS numbers: 61.46.+w, 62.25.+g

The deformation of carbon nanotubes (CNTs) has been the subject of numerous experimental, elastic continuum modeling, and molecular dynamics (MD) studies. The small dimensions of CNTs pose challenges for experimental determination of mechanical behavior and properties. Several experimental studies have attempted to measure the elastic modulus of carbon nanotubes by vibration of individual CNTs or by directly measuring the reaction force for an imposed displacement (e.g., [1–4]) and by nanoindentation of vertically aligned multiwalled carbon nanotube (MWNT) arrays [5]. Most experimental measurements impose some form of bending on the MWNTs and utilize beam theory to reduce data to an elastic modulus. Beam theory treats the nanotube as a homogenous solid tube, but does not take into account any specific structural details of nanotubes, such as the nested tube structure of the MWNT and/or the single-atomic-layer nature of each tube wall. The importance of specific features of CNT structure on its deformation behavior has been documented in several microscopy studies (e.g., [4,6,7]) and investigated in a continuum study by Ru [8]. MWNTs under bending develop reversible periodic wrinkles on the compressive side of the bend (e.g., [4,6,7]). Interwall spacing is preserved during buckling, demonstrating a mechanical effect of the strong normal van der Waals (vdW) interactions present between the walls of MWNTs. The wall-to-wall shear interaction is very compliant and weak [9] compared to the normal vdW stiffness and strength.

Electronic and MD simulations of the structure and deformation of CNTs have been conducted by several investigators (e.g., [10–15]). MD simulations have shown that nanotubes possess an excess internal (strain) energy per carbon atom, relative to an unstrained graphene sheet. The energy exhibits a $1/R^2$ dependence on the tube radius, R, and is insensitive to chirality (e.g., [13–15]). This result is consistent with continuum-level elastic shell theory and indicates that carbon nanotubes contain an initial "internal stress." Fitting results from *ab initio* and MD studies [15] to elastic shell theory, Yakobson *et al.* [11] determined values of the effective Young's modulus and "mechanical" wall thickness that enable shell theory to correctly predict the wall membrane and wall bending stiffnesses of single-wall nanotubes (SWNTs). The surface Poisson ratio extracted from MD simulations is $\nu = 0.19$, the same as the in-plane Poisson ratio of graphite [16]. Later tight-binding simulations [14], local density approximation models [17], and *ab initio* energy calculations [18] confirmed that the strain energy of a deformed SWNT is consistent with shell theory and that the calculations in [11] on the effective modulus and wall thickness were substantially correct. Thus, the wall of a CNT can be modeled as an elastic shell of thickness $t_{\text{wall}} = 0.075$ nm, with effective isotropic elastic constants $E_{\text{wall}} = 4.84$ TPa and $\nu = 0.19$. Effects of using somewhat different (E_{wall}, t_{wall}) pairs are reported in [19].

The cited experimental and modeling results reveal that SWNTs and MWNTs can be successfully modeled based on continuum elastic shell theory [20], provided that four key aspects of the CNT are properly addressed. First, the membrane and bending behaviors of each carbon nanotube wall can be modeled using shell theory with an appropriate set of elastic constants and the corresponding mechanical wall thickness of the shell; here, we use the pairing of elastic properties and the mechanical thickness given above. Second, the initial curvature of a CNT deforms the lattice from a stress-free planar hexagonal graphene structure to a wrapped structure containing an initial internal stress. Here, we impose an initial internal "bending" stress distributed through the thickness of the tube, scaling inversely with the tube radius. Third, surface elements of a CNT wall interact with those of other CNTs, with other portions of itself, and with like substrates via strong vdW interactions. We construct an interaction element whereby the vdW interaction is modeled as an interwall pressure/cohesion dependent on interwall separation distance, as determined by Zhao and Spain [21] from the Lennard-Jones potential of Girifalco *et al.*

[22]; the wall spacing is 0.34 nm. Fourth, the wall-to-wall shear resistance is negligibly small [9] and taken to be zero. These four features were implemented into a novel finite element based continuum shell theory approach [23]. For details on the current implementation, the reader is referred to [19].

The new finite element (FE) based modeling approach is used to simulate the nonlinear mechanical behavior of several MWNTs under bending and compression; results are compared with micrographs. Bending of a MWNT develops characteristic wavelike distortions or wrinkles on the compressive side of the bend. This local wrinkling is a complicated form of buckling, where vdW interactions of neighboring tube walls constrain wrinkling, analogous to the classic problem of buckling on an elastic foundation [24]. Experimental observations (e.g., [4,6,7]) show the effects of the vdW interactions: the wrinkles permeate into the inner walls, with amplitude decreasing monotonically from the outside wall to the inner walls. Here, we simulate the bending of a 14-walled CNT constructed of nested (n, n) tubes, with $n = 5, 10, 15, \ldots, 70$; the outer tube radius is $R = 4.76$ nm. The length of the tube is $L = 15$ nm. A bending angle of $\theta = 0.4$ rad is gradually applied, imposing global curvature $\kappa = \theta/L$; the maximum κ is 0.0133 (1/nm). At one end, each tube section is rigidly rotated while radial and circumferential displacements are constrained; the opposite tube end is a symmetry plane. The total moment versus the global curvature diagram is shown in Fig. 1 for this case, along with several other simulated cases (4-, 8-, and 19-walled CNTs).

Contours of the interwall pressure for the 14-walled CNT are shown in Fig. 2 at selected imposed curvatures, elucidating interwall interactions and the progression of wrinkling. The first deformed configuration, marked (a), corresponds to the onset of buckling; its location on the moment-curvature diagram is indicated in Fig. 1. For any given κ, the peak compressive strain in successive walls increases linearly with respect to wall radius. The outer walls cooperatively buckle at a κ value when local wall bending and vdW potential storage become energetically more favorable than local compressive stretching. Initial buckling occurs with a relatively small axial wavelength, λ; this wavelength will be discussed in more detail below. As the outer layers buckle, vdW interactions develop, opposing relative radial motion of the outer walls. As κ

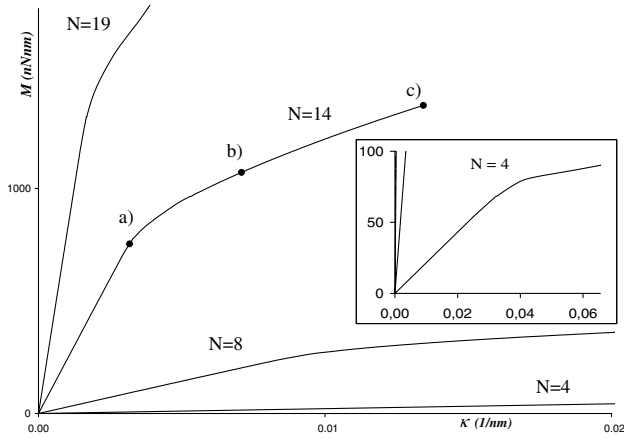

FIG. 1. Pure bending of N-walled carbon nanotubes constructed of nested (n, n) tubes: total moment, the sum of the moments acting on all N tube walls, versus global curvature.

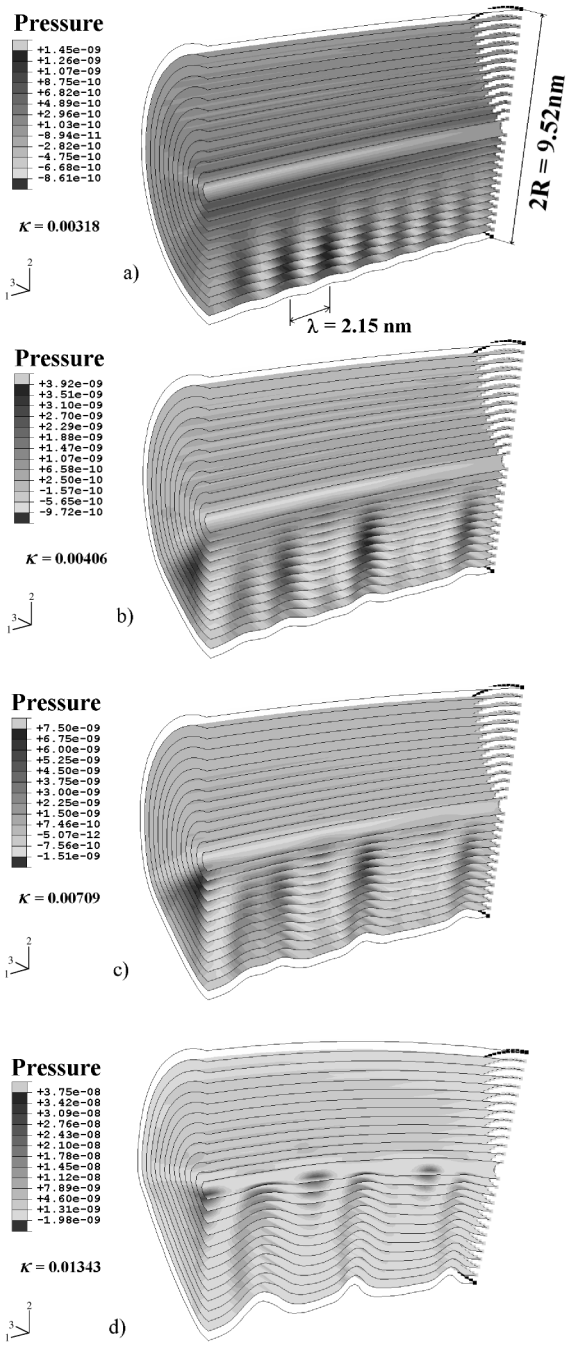

FIG. 2. FE bending simulation of a 14-walled MWNT model at indicated curvatures, κ, in 1/nm. Distribution of the interwall pressure in N/nm^2 at the locations (a), (b), (c), and (d) of Fig. 1.

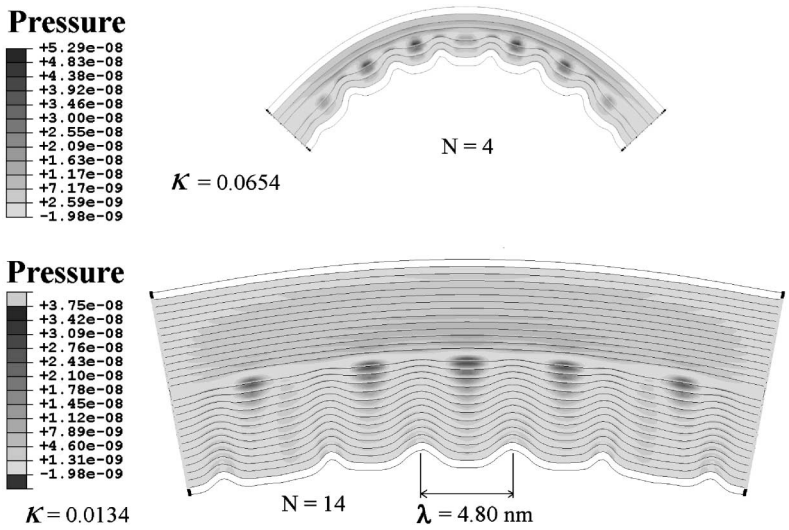

FIG. 3. Distribution of the interwall pressure, in N/nm^2, at the final imposed curvature, in 1/nm, of 4- and 14-walled CNTs.

increases, the outer tubes attempt to increase their wrinkling amplitude, but the vdW forces resist the developing interwall radial separation; instead, the wavelength λ increases with a further increase in global curvature [Figs. 2(b) and 2(c)], ultimately resulting in a buckling wavelength much longer than that initially observed at the buckling onset.

Furthermore, the wavelength evolution is associated with a sharpening of the intrusions, as is also observed experimentally [4,6]. This sharpening results from the nonlinear and directional nature of the vdW interactions. As κ increases further [Fig. 2(d)], the wrinkle permeates to the innermost wall; no noticeable changes in interwall spacings are observed. The 14-walled CNT simulation compares well with the TEM image of Bower *et al.* [[6], Fig. 2(b)] in terms of both final λ and deformed configuration. The same progression is observed in all of the MWNT cases simulated. In our simulations the local radius of curvature at the deepest kink is never smaller than 0.27 nm. Thus, no complete and irreversible sp^2 to sp^3 transition should take place [25,26].

Figure 3 shows the final deformed configurations for a 4-walled (n, n) CNT (with $n = 5$, 10, 15, and 20) and the 14-walled CNT discussed. Depiction of axial sections of the models and their images reflected across the symmetry plane provides a clearer view of the characteristic wavelike distortion on the area under compression; for the 14-walled tube, the final axial wavelength in the central section is $\lambda = 4.80$ nm, considerably larger than the initial value of 2.15 nm shown in Fig. 2(a).

Thin shell theory predicts the wrinkling wavelength, λ, to scale by $(Rh)^{1/2}$, where R is the tube outer radius and h is the shell thickness [24]. For a material with $\nu = 0.19$, shell theory gives the wavelength of local buckling in an isolated tube as $\lambda = 3.4(Rh)^{1/2}$. Figure 4 plots various model (shell theory and the new FE based model) and experimental results of λ vs $(Rh)^{1/2}$, where both lengths have been normalized by $\xi = 0.24$ nm, the height of the hexagonal graphene lattice cell . As shown in Fig. 4, taking h to be the thickness of the outer wall (t_{wall}), the initial λ computed by the new FE based approach (open triangles) is in excellent agreement with thin shell theory (which considers only a single thin tube). As discussed earlier, the final λ greatly exceeds its initial value for all cases; this results in the much steeper-sloped line shown in Fig. 4 (open diamonds). Using TEM, Bower *et al.* [6] observed buckling wavelengths for various bent MWNTs in polymer matrix composites. Figure 4 shows the experimentally observed wavelengths, where Bower (open circles) took h to be the total tube thickness; additional experimental results [7] are plotted with filled squares. In Fig. 4, final λ values computed in the FE based simulations (filled triangles) are again reported, but this time with h taken to be the total tube thickness. The agreement of the new computational results with experiments is remarkable.

Finally, we present results from FE simulations of axial compression of the 4-walled and 14-walled CNTs

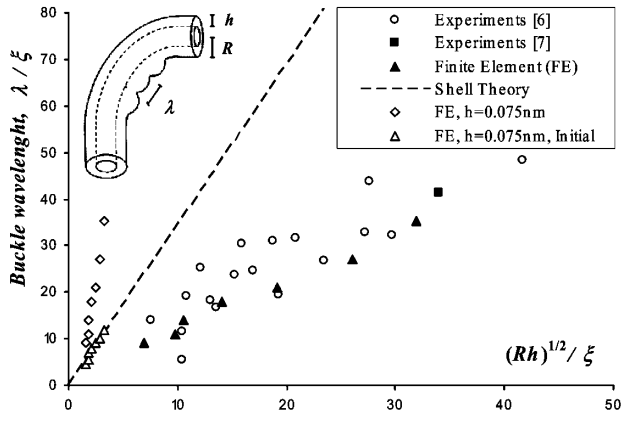

FIG. 4. Normalized axial buckling wavelengths, λ, of the buckled MWNTs versus a normalized geometric dimension of the nanotubes. Here $\xi = 0.24$ nm, R is the outer radius and h is either total MWNT thickness or SWNT effective thickness 0.075 nm (open diamonds and open triangles).

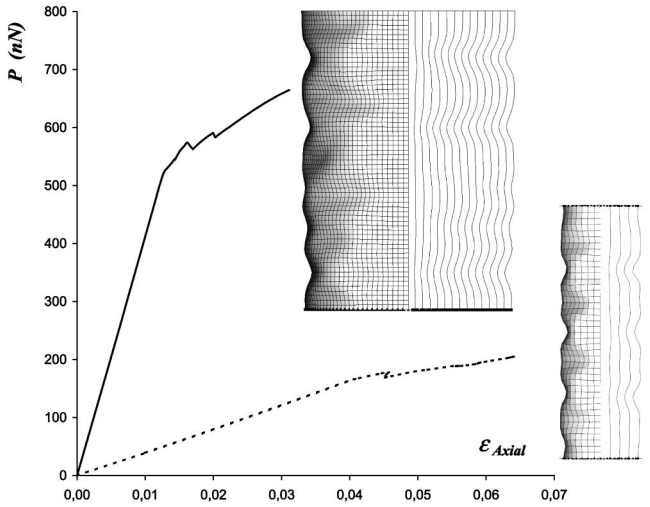

FIG. 5. Axial compression of 4-walled and 14-walled carbon nanotubes; load versus macroscopic axial strain, $\varepsilon_{\text{axial}} = \Delta/L$. The deformed configurations at the final stage of each simulation are shown.

analyzed above. In-plane motion at one end is constrained as uniform shortening, Δ, is imposed; the other tube end is again a symmetry plane. Figure 5 shows the axial load versus macroscopic strain plots, together with the deformed configurations at the final stage of each simulation. Because of the vdW interactions tending to preserve interwall spacings and the presence of inner walls that are very stiff to radial motion and consequent circumferential stretching, axially symmetric buckling is not observed. Local buckling progressed during axial compression in much the same manner as seen in bending: initial buckling occurs at a small axial wavelength; the wavelength gradually increases with continued deformation until reaching a final wavelength; the final wavelength then permeates through to the inner walls. The initial and final wavelengths for the axial compression cases correspond to those obtained during bending, thus emphasizing the local buckling nature of this wrinkling phenomenon in MWNTs.

In summary, a methodology for constructing FE based shell theory models of carbon nanotubes has been established. The technique enables investigation of the mechanics of geometrically nonlinear deformations, including the onset and evolution of buckling in MWNTs. The technique can also be utilized to study other phenomena involving the deformation of carbon nanotubes due to competing effects of tube bending stiffness and vdW interaction (see [19]) as observed in tube-substrate and tube-tube interactions.

This research was funded in part by the Cambridge-MIT Institute Project on Carbon Nanotube Enabled Materials, and in part by the AFOSR DURINT on Microstructure, Processing and Mechanical Performance of Polymer Nanocomposites (Contract No. F49620-01-1-0477).

*Corresponding author.
Email address: dmparks@mit.edu

[1] M. M. Treacy, T.W. Ebbesen, and J. M. Gibson, Nature (London) **381**, 678 (1996).
[2] M. F. Yu, O. Lourie, M. J. Dyer, K. Moloni, T. F. Kelly, and R. S. Ruoff, Science **287**, 637 (2000).
[3] E.W. Wong, P. E. Sheehan, and C. M. Lieber, Science **277**, 1971 (1997).
[4] P. Poncharal, Z. L. Wang, D. Ugarte, and W. A. de Heer, Science **283**, 1513 (1999).
[5] H. J. Qi, K. B. K. Teo, K. Lau, M. C. Boyce, W. I. Milne, J. Robertson, and K. K. Gleason, J. Mech. Phys. Solids (to be published).
[6] C. Bower, R. Rosen, L. Jin, J. Han, and O. Zhou, Appl. Phys. Lett. **74**, 3317 (1999).
[7] O. Lourie, D. M. Cox, and H. D. Wagner, Phys. Rev. Lett. **81**, 1638 (1998).
[8] C. Q. Ru, J. Appl. Phys. **87**, 7227 (2000).
[9] J. Cumings and A. Zettl, Science **289**, 602 (2000).
[10] S. Iijima, C. Brabec, A. Maiti, and J. Bernholc, J. Chem. Phys. **104**, 2089 (1996).
[11] B. I. Yakobson, C. J. Brabec, and J. Bernholc, Phys. Rev. Lett. **76**, 2511 (1996).
[12] M. Buongiorno Nardelli, B. I. Yakobson, and J. Bernholc, Phys. Rev. B **57**, R4277 (1998).
[13] D. Sanchez-Portal, E. Artacho, J. M. Soler, A. Rubio, and P. Ordejon, Phys. Rev. B **59**, 12 678 (1999).
[14] Xin Zhou, Jianjun Zhou, and Zhong-can Ou-Yang, Phys. Rev. B **62**, 13 692 (2000).
[15] D. H. Robertson, D.W. Brenner, and J.W. Mintmire, Phys. Rev. B **45**, 12 592 (1992).
[16] B. Kelly, *Physics of Graphite* (Applied Science Publishers, London, 1981).
[17] Z. C. Tu and Zhong-can Ou-Yang, Phys. Rev. B **65**, 233407 (2002).
[18] K. N. Kudin, G. E. Scuseria, and B. I. Yakobson, Phys. Rev. B **64**, 235406 (2001).
[19] A. Pantano, D. M. Parks, and M. C. Boyce, J. Mech. Phys. Solids (to be published).
[20] Treatises on elastic shell theory include A. E. H. Love, *A Treatise on the Mathematical Theory of Elasticity* (Dover, New York, 1944), 4th ed.; V.V. Novozhilov, *The Theory of Thin Elastic Shells* (Noordhoff, Groningen, 1959).
[21] Y. X. Zhao and I. L. Spain, Phys. Rev. B **40**, 993 (1989).
[22] L. A. Girifalco and R. A. Lad, J. Chem. Phys. **25**, 693 (1956).
[23] Treatises on nonlinear continuum and structural mechanics via finite element methods include T. Belytschko, W. K. Liu, and B. Moran, *Nonlinear Finite Elements for Continua and Structures* (John Wiley, New York, 2000); K. J. Bathe, *Finite Element Procedures* (Prentice-Hall, Englewood Cliffs, NJ, 1995), 2nd ed.
[24] S. Timoshenko, *Theory of Elastic Stability* (McGraw-Hill, New York, 1936).
[25] A. Maiti, Chem. Phys. Lett. **331**, 21–25 (2000).
[26] T.W. Ebbesen and T. Takada, Carbon **33**, 973–978 (1995).